KLC3 activates PI3K/AKT signaling and promotes ovarian cancer cell proliferation and migration through COL3A1

JING YANG[1*], RONGXIA HE[2*], XIAOLING ZHANG[3], XING WANG[1], MIN LIU[2], XIAOLONG LIU[1] and YULAN LI[1,4]

[1]The First School of Clinical Medical, Lanzhou University, Lanzhou, Gansu 730000, P.R. China; [2]Department of Obstetrics, Lanzhou University Second Hospital, Lanzhou, Gansu 730000, P.R. China; [3]Department of Pathology, Gansu Provincial Hospital, Lanzhou, Gansu 730000, P.R. China; [4]Department of Anesthesiology, The First Hospital of Lanzhou University, Lanzhou, Gansu 730000, P.R. China

Received November 19, 2024; Accepted March 13, 2025

DOI: 10.3892/or.2025.8900

Abstract. Ovarian cancer (OC) is a prevalent malignancy; however, the role of kinesin light chain 3 (KLC3) in OC remains unclear. The present study conducted a comprehensive investigation of KLC3 using bioinformatics analysis, as well as *in vitro* and *in vivo* experiments. The findings revealed that KLC3 expression was significantly upregulated in the OC group compared with that in the normal group, and high KLC3 expression in patients with OC was associated with a poorer overall survival. Functional studies demonstrated that targeting KLC3 effectively suppressed the proliferation, migration, epithelial-mesenchymal transition and DNA damage resistance of OC cells *in vitro*, while also inhibiting tumor growth *in vivo*, underscoring the pivotal role of KLC3 in tumor progression and metastasis. Additionally, RNA-sequencing analysis identified collagen type III α1 (COL3A1) as a potential downstream gene cooperating with KLC3 to promote the occurrence and development of OC through the PI3K/AKT signaling pathway. Rescue experiments revealed that the KLC3 knockdown-induced suppression of the malignant phenotype could be partially reversed by overexpression of COL3A1. In summary, the present findings demonstrated that KLC3 acts as an oncogene by influencing COL3A1 expression to promote the proliferation and migration of OC cells *in vivo* and *in vitro*.

Correspondence to: Professor Yulan Li, The First School of Clinical Medical, Lanzhou University, 1 Donggang West Road, Lanzhou, Gansu 730000, P.R. China
E-mail: liyul@lzu.edu.cn

*Contributed equally

Key words: ovarian cancer, kinesin light chain 3, collagen type III α1, PI3K/AKT signaling pathway

Introduction

Ovarian cancer (OC) is the most prevalent gynecological cancer worldwide, posing a significant threat to women's health (1). Globally, the primary factors contributing to OC-associated mortality include delayed diagnosis, chemotherapy resistance, high metastasis rates and heterogeneity (2). Despite the ongoing development of novel targeted therapies and chemotherapeutic drugs, the prognosis for OC remains unfavorable due to resistance and recurrence (2). Therefore, it is imperative to explore the pathogenic mechanisms of OC and to develop early diagnostic indicators.

Kinesins are a class of evolutionarily conserved motor proteins that generate motive force by hydrolyzing ATP and binding to microtubules, thus serving an important role in various aspects of intracellular transport and widely participating in various physiological processes, including embryonic development, axon transport and cell division (3). Previous studies have shown that most kinesins are expressed at higher levels in tumors compared with those in normal tissues (4-12). Kinesins consist of the kinesin heavy chain and the kinesin light chain (KLC), with KLCs generally considered to participate in cargo binding and regulation of motor protein activity. There are four subtypes of KLCs: KLC1, KLC2, KLC3 and KLC4 (13). In lung cancer, it has been demonstrated that KLC1, KLC2 and KLC4 are associated with drug resistance and poor prognosis (5-7). In OC, multiple members of the kinesin family are considered to promote OC proliferation and migration, while being associated with poor prognosis (8-12). However, there have been limited reports on the pathways involved and the precise mechanisms related to KLC3 in OC occurrence.

PI3K/AKT is an important intracellular signaling pathway, which is involved in cell cycle regulation, proliferation, glycation, epithelial-mesenchymal transition (EMT), cancer development, tumor recurrence and drug resistance (14). The development and application of small molecule inhibitors targeting this pathway have shown promising clinical efficacy (15). Publicly available data have indicated that ~70% of patients with OC exhibit activation of the PI3K/AKT pathway. In addition, there is strong preclinical and clinical evidence for

potent PI3K/AKT pathway inhibitors in OC; however, there are currently no Food and Drug Administration-approved inhibitors for the treatment of OC (15,16).

The aim of the current study was to investigate the expression of KLC3 in OC tissue and its role in the proliferation and migration of OC cells.

Materials and methods

Analysis of KLC3 expression and prognosis using online databases. The Gene Expression Profiling Interactive Analysis (GEPIA; http://gepia.cancer-pku.cn/) and Gene Expression Omnibus (GEO; https://www.ncbi.nlm.nih.gov/geo/) databases were utilized to assess the mRNA expression levels of KLC3 in OC. The Cancer Genome Atlas (TCGA) TCGA-OV data (https://www.cancer.gov/ccg/research/genome-sequencing/tcga) and the Genotype-Tissue Expression normal ovarian tissue data (https://commonfund.nih.gov/genotype-tissue-expression-gtex) were obtained from the GEPIA, and the GSE12470 (17) and GSE18520 (18) datasets were obtained from the GEO. Tumor samples in all databases were not matched to normal samples, the normal samples were from healthy individuals. Additionally, the Kaplan-Meier plotter (http://kmplot.com/analysis/) was employed to investigate the association between KLC3 expression and the prognosis of patients with OC.

Clinical specimens and cell lines. Five patients with OC who underwent surgery at The First Hospital of Lanzhou University (Lanzhou, China) between June 2022 and November 2022, along with five normal ovarian samples (healthy controls), were collected for western blot analysis. The average age of the healthy control group for western blotting and IHC was 60 years old, including women aged between 55 and 62 years old. Ovarian samples were obtained following hysterectomy for benign gynecological diseases, such as abnormal uterine bleeding, adenomyosis, uterine fibroids and uterine abscess. Furthermore, 48 OC tissues and 10 normal tissues collected from healthy controls were obtained between January 2020 and January 2023 were used for immunohistochemistry (IHC). Table I provides the basic features of the patients, and International Federation of Gynecology and Obstetrics staging was used in all patients (19). All patients were diagnosed with OC through pathological examination and their clinical data were recorded. None of the patients had received targeted therapy, chemotherapy or radiotherapy prior to surgery. The present study was approved by the Ethics Committee of The First Hospital of Lanzhou University (approval no. LDYYLL-2019-279), and all tissues involved in the present study were stored in the Biobank of The First Hospital of Lanzhou University, where all samples were stored with the consent of patients. The medical records were available for the participants, and all participants provided written informed consent and their samples were anonymized. The current study was conducted in compliance with the International Conference on Harmonization guidelines for Good Clinical Practice (20) and the 2013 Declaration of Helsinki. TheSKOV3 and A2780 human OC cell lines used in the present study were sourced from the Cell Resource Center, Institute of Basic Medicine, Chinese Academy of Medical Sciences. All cells were cultured in DMEM (Gibco; Thermo Fisher Scientific, Inc.) supplemented with 10% FBS, 10 mg/ml streptomycin, 10,000 U/ml penicillin and 25 μg/ml amphotericin B (all from Gibco; Thermo Fisher Scientific, Inc.) at 37˚C and 5% CO_2.

Table I. Basic characteristics of patients.

Characteristic	Number (n=48)
Age, years	50.3±8.6
FIGO stage	
I-II	21 (43.7%)
III-IV	27 (56.3%)
Lymph node invasion	
Yes	16 (33.3%)
No	32 (66.7%)
Histological grade	
G1	4 (8.3%)
G2	7 (14.6%)
G3	37 (77.1%)

Data are presented as the mean ± standard deviation or number (%). FIGO, International Federation of Gynecology and Obstetrics.

Cell transduction and transfection. The lentivirus design and packaging were provided by Shanghai GeneChem Co., Ltd. The experimental group was divided into two groups: The knockdown group and the overexpression group. The knockdown groups included the short hairpin (sh)RNA negative control (NC), shKLC3-64#, shKLC3-65# and shKLC3-66# groups, and the overexpression groups included the Vector (empty vector) and KLC3 groups. All SKOV3 and A2780 cells were cultured in a constant temperature incubator at 37˚C and 5% CO_2. According to the transduction instructions, KLC3 knockdown plasmids with a pPLK GFP+Puro plasmid backbone were provided by Shanghai GeneChem Co., Ltd. The 2nd generation system was used for plasmid packaging. A total of 1.5 μg knockdown plasmids, 1 μg pCMV-VSV-G and 0.5 μg pCAG-dR8.9 (both from Beyotime Institute of Biotechnology) were transfected into 293T cells (The Cell Bank of Type Culture Collection of The Chinese Academy of Sciences) in 6-well plates using Lipofectamine® 3000 transfection reagent (Invitrogen; Thermo Fisher Scientific, Inc.) according to the manufacturer's instructions at 37˚C. Lentiviral particles were harvested 48 h post-transfection, followed by infection of SKOV3 OC cells for 24 h. Cells (30% confluence) were seeded in cell culture dishes and were infected with lentiviral plasmids at multiplicity of infection (MOI) of 10. At 37˚C and screening of the cells for 7 days with medium containing 2 μg/ml puromycin (Beyotime Institute of Biotechnology). The target sequences of the knockdown lentiviral plasmids were as follows: shNC, 5'-TGTCGCGGTAAGTGCCTCATA-3'; shKLC3-64#, 5'-CAACAACTTGGCTGTCCTCTA-3', shKLC3-65#, 5'-GACCCTGCATAACCTCGTGAT-3' and shKLC3-66#, 5'-GCCACAGACCTTCTCCATGAT-3'.

In order to construct a plasmid for overexpressing KLC3, full-length human KLC3 cDNA was first cloned into a p-Enter plasmid (Shanghai GeneChem Co., Ltd.). The p-Enter-KLC3 construct was then recombined into a Lenti-CMV expression vector to generate the final Lenti-CMV-KLC3 plasmid for lentiviral packaging. Lentiviral particles were produced by co-transfecting the Lenti-CMV-KLC3 or Lenti-CMV-vector (negative control) plasmids with the packaging plasmid pSPAX2 and the envelope plasmid pMD2.G into 293T cells (~70% confluence in 6-well plates) using Lipofectamine 3000 at 37˚C, according to the manufacturer's protocol. After 6 h of transfection, the medium was replaced with fresh complete medium. For lentiviral transfection, the ratio of lentiviral plasmid to packaging and envelope plasmids was Lenti-CMV-KLC3/Lenti-CMV-vector: pSPAX2 (packaging plasmid): pMD2G (envelope plasmid)=1:1:0.5 μg. After 36 h of culture, the virus was harvested from the supernatant and concentrated with lenti-X-concentrator (Shanghai GeneChem Co., Ltd.), and then added to A2780 cells along with 5 μg/ml polybrene (Beyotime Institute of Biotechnology). Cells (30% confluence) were seeded in cell culture dishes and were infected with lentiviral plasmids at a MOI of 15 at 37˚C. The cells were initially selected with medium containing 2.0 μg/ml puromycin (Beyotime Institute of Biotechnology) for 48 h. The medium was then replaced with medium containing 5.0 μg/ml puromycin, which was used for maintenance over a 7-day period to establish stable cell lines. Western blotting was employed to verify the infection efficiency, with the Lenti-CMV-vector serving as the control.

For COL3A1 overexpression, SKOV3 cells were transfected with a pcDNA3.1 plasmid (2 μg) encoding COL3A1 cDNA, whereas empty vectors served as the NC group. All plasmids were synthesized by Beijing Sino Technology Co. Ltd. The SKOV3 cells were seeded in 6-well plates at a density of $1x10^6$/well were transfected with the aforementioned plasmids (10 μg) using Lipofectamine 2000 for 48 h at 37˚C according to the manufacturer's instructions. The cells were collected for subsequent experiments 48 h post-transfection. In addition, in the cells with both KLC3 knockdown and COL3A1 overexpression, SKOV3 cells were transfected for 48 h with the COL3A1 plasmid after infection with shKLC3. In addition, western blotting was used to verify the transfection efficiency.

Reverse transcription-quantitative PCR (RT-qPCR). TRIzol® reagent (Invitrogen; Thermo Fisher Scientific, Inc.) was used to extract total RNA from SKOV3 and A2780 cells, A NanoDrop 2000 spectrophotometer was used to measure the RNA concentration, and cDNA was synthesized by RT of 1 μg total RNA according to the manufacturer's protocol of the RT kit (cat. no. R233-01; Vazyme Biotech Co., Ltd.). A qPCR machine was used to amplify cDNA using the SYBR Green qPCR Mix (cat. no. Q711-02; Vazyme Biotech Co., Ltd.). The thermocycling conditions for amplification were as follows: 95˚C for 5 min, followed by 40 cycles at 95˚C for 10 sec, 60˚C for 30 sec and a final step at 95˚C for 15 sec, 60˚C for 60 sec and 95˚C for 15 sec. GAPDH was used as an internal control. Subsequently, the $2^{-\Delta\Delta Cq}$ method was used to analyze the gene expression data (21). β-actin was used as an internal control. The primer sequences were as follows: β-actin, forward 5'-GCGTGACATTAAGGAGAAGC-3', reverse 5'-CCACGTCACACTTCATGATGG-3'; KLC3, forward 5'-CTCAACATCCTGGCGCTGGT-3', reverse 5'-TCCCGGTAACGCCCACGCTTC-3; CXCL12, forward 5'-TGCCCTTCAGATTGTAGCCC-3', reverse 5'-CTGTAAGGGTTCCTCAGGCG-3'; IGFL3, forward 5'-TGCTGTCCCGAGTCTTTTGG-3', reverse 5'-GTGCCTCCTGTTCCTGGTA-3'; COL3A1, forward 5'-TAAAGGCGAAATGGGTCCCG-3', reverse 5'-GGCACCATTCTTACCAGGCT-3'; COL1A2, forward 5'-GAGGAGAGCCTGGCAACATT-3', reverse 5'TCCACCTTGAACACCCTGTG-3'; TENM2, forward 5'-CAAAGAGTGTCGCTACACAAGC-3', reverse 5'-TCCTGCTGTCATGGTCATAGG-3'; CREB3L1, forward 5'-TGGAGAATGCCAACAGGACC-3', reverse 5'-CCAGCACCAGAACAAAGCAC-3'; MMP13, forward 5'-CAGTTTGCAGAGCGCTACCT-3', reverse 5'-TTCTCGGAGCCTCTCAGTCA-3'; IGFBP5, forward 5'-ACAAGAGAAAGCAGTGCAAACC-3', reverse 5'-CGTCAACGTACTCCATGCCT-3'; SLC14A1, forward 5'-AGCCAGCTAGAGTGGTCTTT-3', reverse 5'-TCCAAACAGGACCATGACGG-3'; SPARC, forward 5'-TTCGGCATCAAGCAGAAGGAT-3', reverse 5'-TTAGCACCTTGTCTCCAGGC-3'.

Xenograft model. A total of 12 4-week-old female BALB/c nude mice (weight, 15-16 g) were purchased from Beijing Vital River Laboratory Animal Technology Co., Ltd. The mice were housed in the animal facility under standard conditions, with a controlled temperature of 25±2˚C and humidity of 55±5%, under a 12-h light/dark cycle, with free access to water and food. Each mouse received a subcutaneous injection of 100 μl ($5x10^6$) cell suspension into the right flank with shNC-infected SKOV3 cells, shKLC3-infected SKOV3 cells, Vector-infected A2780 cells or KLC3-overexpressing A2780 cells. The study was terminated based on tumor volume (~1,500 mm^3) as the humane endpoint. Mice injected with shNC-infected SKOV3 cells and shKLC3-infected SKOV3 cells were sacrificed on day 24, whereas mice injected with Vector-infected A2780 cells and KLC3-overexpressing A2780 cells were sacrificed on day 21. Notably, no mice succumbed before reaching the humane endpoint criteria. Tumor volume was measured twice per week using electronic calipers and the animals were weighed five times per week. At the end of the study, mice were euthanized by CO_2 asphyxiation (30% vol/min) followed by cervical dislocation as noted in the IACUC-approved protocol, and the tumors were excised, weighed and cut in half. No analgesics were administered during the study since flank tumor studies are considered painless. Animal experiments were approved by the Animal Experimental Ethics Committee of The First Hospital of Lanzhou University (approval no. LDYYLL-2023-495).

IHC. Samples were fixed in 10% neutral formalin fixative solution (BBI Solutions) embedded in paraffin at room temperature overnight, and divided into 3-μm sections, which were deparaffinized with xylene and then rehydrated with a succession of decreasing alcohol concentrations (100, 95, 85, 70 and 50% ethanol). Tissue sections were then placed in antigen retrieval buffer (pH 9.0; Wuhan Servicebio Technology Co., Ltd.) in a microwave oven on medium power for 8 min until boiling, then cooled for 8 min and switched to medium-low power for 7 min. After natural cooling, the slides were placed in PBS

(pH 7.4; Wuhan Servicebio Technology Co., Ltd.) and washed three times on a destaining shaker. Subsequently, 3% hydrogen peroxide solution was added to the sample at room temperature for 25 min to block endogenous peroxidase, followed by blocking with 3% BSA (Sangon Biotech Co., Ltd.) at room temperature for 30 min. The histological sections were then incubated at 4˚C overnight with rabbit anti-KLC3 antibody (1:200; cat. no. ab180523; Abcam) and anti-PCNA antibody (1:200; cat. no. 10205-2-AP; Proteintech Group, Inc.), and with a horseradish peroxidase-conjugated goat anti-rabbit IgG secondary antibody (1:200; cat. no. SA00001-2; Proteintech Group, Inc.) at 37˚C for 30 min. Sections were then counterstained with 0.1% hematoxylin (Boster Biological Technology) at room temperature for 2 min and were stained with the chromogen DAB (Boster Biological Technology). With an objective magnification of x200 or x400, histological images were captured using a light microscope (cat. no. AE2000; Motic Incorporation, Ltd.). A total of 10 normal ovarian tissue samples and 48 OC tissue samples, as well as mouse tumor tissues were selected for assessing expression levels. The IHC scores were independently evaluated by two pathologists. Staining intensity was categorized as 0, no staining; 1, weak staining; 2, moderate staining; and 3, strong staining. Based on the extent of brown staining, the stained area was divided into percentages ranging from 1 to 99%. Finally, the staining intensity and stained area were each multiplied by 100. The patients were divided into two groups, high and low expression, according to the median value.

Cell Counting Kit (CCK)-8 assay. For the CCK-8 assay, wild-type and infected cells were seeded in 96-well plates and incubated with CCK-8 Reagent (Shanghai Yeasen Biotechnology Co., Ltd.) for 2 h over 5 consecutive days. The CCK-8 reagent was added for a 2-h incubation period. Absorbance at 450 nm was subsequently measured using a microplate reader.

Colony formation assay. Wild-type and infected/transfected cells were seeded at a density of 500 cells/well in 6-well plates. After 14 days, the cells were stained with 10% Giemsa (Beijing Biotopped Technology Co., Ltd.) at room temperature for 10 min after being fixed with methanol at room temperature for 30 min. To assess the colony formation capacity of the cells, visible colonies were counted. A dense conglomerate of cells was regarded as a colony when the number of cells exceeded 50. ImageJ software [Fiji (https://imagej.net/software/fiji/downloads) (National Institutes of Health)] was used to count the number of colonies. This experiment was repeated three times.

Comet assay. Cells were cultured in 6-well plates until they reached ~30% confluence. The transduced cells were subsequently trypsinized and collected by centrifugation at 1,200 x g for 5 min at 4˚C, forming a compact pellet. After washing, the cells were resuspended in 200 μl ice-cold 1X PBS. Subsequently, the cell suspension was carefully mixed at a ratio of 1:10 with low melting point agarose maintained at 42˚C and was promptly pipetted onto the designated CometSlide™ area (Shanghai Yeasen Biotechnology Co., Ltd.). Slides were incubated in the dark at 4˚C for 30 min, followed by immersion in chilled lysis solution (Trevigen, Inc.; Bio-Techne) at 4˚C for 30 min. The slides were then incubated in alkaline unwinding buffer (0.3 N NaOH, 1 mM EDTA) at room temperature for 30 min. The slides were then transferred to a horizontal electrophoresis chamber and subjected to electrophoresis using buffer (0.3 N NaOH, 1 mM EDTA) at an electric field strength of 1 $V \cdot cm^{-1}$ for 20 min. Following electrophoresis, the samples were dried and stained with ethidium bromide. The comet tails were visualized under a DM 2500 fluorescence microscope (Leica Microsystems GmbH) and were quantified using Komet 5.5 software (Andor Technology Ltd.). A minimum of 50 cells were analyzed per treatment condition. All experiments were conducted independently at least three times.

Wound healing assay. Infected/transfected cells were cultured to ~90% confluence in 12-well plates and a wound was introduced using a sterile 200-μl pipette tip. After washing twice with PBS, cells were cultured in DMEM/F12 without FBS for 48 h. Cell images were obtained using fluorescence microscopy (IX73; Olympus Corporation). Wound sizes were measured with ImageJ 1.5.2a software and were calculated as a percentage (from 0 to 24 h).

Transwell migration assay. Transwell migration assays were conducted using 24-well plates fitted with membranes containing 8-μm pores (Corning, Inc.). Cells were seeded on the upper chamber without serum at a density of $2x10^4$ cells/well, whereas complete medium supplemented with 10% FBS, 10 mg/ml streptomycin, 10,000 U/ml penicillin and 25 μg/ml amphotericin B was added to the lower chamber. After a 24-h incubation period at 37˚C, the cells were removed from the upper chamber using a cotton swab followed by fixation with 4% formaldehyde at room temperature for 30 min and staining with Giemsa solution at room temperature for 15 min. The assessment of migration involved counting cell numbers in 10 random fields under a light microscope (Leica Microsystems, Inc.); this process was repeated three times for accuracy and consistency.

Apoptosis assay. For the apoptosis assay, the cells were harvested, washed with PBS, suspended in binding buffer and sequentially stained with the Annexin V-FITC Detection Kit (Roche Applied Science) according to the manufacturer's protocol. Subsequently, apoptotic cells were detected using a FacsCalibur flow cytometer (BD Biosciences), and the results were analyzed using CellQuest version 3.3 software (BD Biosciences). Each experiment was performed in triplicate.

Western blotting. Total proteins were extracted from cells and tissues using RIPA lysis buffer and PMSF at a ratio of 1:100 (Beyotime Institute of Biotechnology). Phosphorylated proteins were extracted separately with the addition of phosphatase inhibitors (Biosharp Life Sciences). The protein levels were quantified using a BCA assay kit. Subsequently, an equal volume of protein mixture (30 μg) was pipetted into the wells of the gel matrix (containing 30% acrylamide), and the electrical potential was fixed at 120 volts for the purpose of conducting gel electrophoresis. After a 30-min transfer, the PVDF membrane was immersed in a solution of 5% non-fat

milk powder and blocked for 2 h at 25˚C. Subsequently, membranes were washed three times with TBS-0.1% Tween 20 (TBST), followed by incubation with the primary antibodies overnight at 4˚C, three further washes with TBST and incubation with a HRP-conjugated secondary antibody (anti-rabbit IgG; 1:5,000; cat. no. GTX213110; GeneTex, Inc.) for 2 h at 25˚C. Chemiluminescent solution was then added for 10 sec for visualization. The following primary antibodies were used: KLC3 (1:1,000; cat. no. ab180523), E-cadherin (1:10,000; cat. no. ab40772), N-cadherin (1:10,000; cat. no. ab76011), Vimentin (1:5,000; cat. no. ab92547), Snail (1:1,000; cat. no. ab216347), GAPDH (1:5,000; cat. no. ab8245) and α-tubulin (1:10,000; cat. no. ab7291) (all from Abcam); PALB2 (1:2,000; cat. no. 14340-1-AP), XRCC1 (1:1,000; cat. no. 21468-1-AP), XRCC2 (1:20,000; cat. no. 20285-1-AP) and COL3A1 (1:1,000; cat. no. 22734-1-AP) (all from Proteintech Group, Inc.); AKT (1:1,000; cat. no. 9272), PI3K (1:1,000; cat. no. 4292), phosphorylated (p-)AKT (1:1,000; cat. no. 4060) and p85α (also known as p-PI3K; 1:1,000; cat. no. 4228) (all from Cell Signaling Technology, Inc.). Protein visualization was achieved using a highly sensitive ECL substrate kit (Beyotime Institute of Biotechnology). All results were normalized to the internal reference proteins GAPDH and tubulin. Densitometric analysis was carried out using ImageJ 1.5.2a software.

RNA-sequencing (RNA-seq). Total RNA was extracted from SKOV3 cells infected with shKLC3 and shNC using a RNeasy Mini Kit (Qiagen, Inc.), and RNA quality was assessed using an Agilent Bioanalyzer (Agilent Technologies, Inc.). Samples with RNA integrity number >7.0 were used for library preparation. A total of 4 μg DNase-treated RNA from each sample was used to construct cDNA libraries using the TruSeq Stranded Total RNA Library Prep Kit (cat. no. 20020597; Illumina, Inc.), according to the manufacturer's protocol. RNA was fragmented and subjected to two rounds of cDNA synthesis and adapter ligation. Libraries were quantified using qPCR (concentration >2 nM) and qualified using an Agilent 2100 Bioanalyzer. Paired-end 100 bp reads were generated on the Illumina NovaSeq 6000 and HiSeq X Ten platforms (NovaSeq 6000 S1 Reagent Kit, 300 cycles; cat. no. 20012863-1; Illumina, Inc.). High-quality reads were obtained by trimming adapters and filtering low-quality reads. Read alignment and differential gene expression analysis were performed using the DESeq2 package (v1.26.0; https://github.com/thelovelab/DESeq2), and genes with a false discovery rate-adjusted P-value (q-value) <0.05 were considered significantly differentially expressed.

Bioinformatics analyses. Multivariate and principal component analyses were performed using the ClustVis online tool (https://github.com/fw1121/ClustVis). Functional enrichment analysis was performed using Metascape (https://metascape.org/gp/index.html#/main/step1) (22). Metascape pathway enrichment analysis uses Kyoto Encyclopedia of Genes and Genomes (https://www.genome.jp/kegg/kegg_ja.html), Reactome (https://reactome.org/) and MSigDB (https://www.gsea-msigdb.org/gsea/msigdb). Statistical significance of gene overrepresentation was assessed using a hypergeometric test (Fisher's exact test), followed by Bonferroni correction for multiple comparisons. Heatmaps and volcano plots were generated using TBtools (v 1.055; https://github.com/CJ-Chen/TBtools/releases).

Co-immunoprecipitation (co-IP). Cells were lysed with 250 μl NP-40 lysis buffer (cat. no. P0013F; Beyotime Institute of Biotechnology) for 30 min on ice and then centrifuged at 16.2 x g and 4˚C for 10 min to remove cell fragments. The protein lysate (200 μl), bound to 25 μl magnetic beads (cat. no. 88802; Thermo Fisher Scientific, Inc.) with anti-KLC3 (1:50; cat. no. ab180523; Abcam), anti- COL3A1 (1:50; cat. no. 22734-1-AP; Proteintech Group, Inc.) or IgG (1:200; cat. no. 10284-1-AP; Proteintech Group, Inc.) antibodies, was incubated overnight at 4˚C. The next day, the magnetic beads were adsorbed using a magnetic grate and washed with lysis buffer (Thermo Fisher Scientific, Inc.). The lysis buffer was transferred to the newly washed column and incubated at 4˚C for 2 h. After incubation, the supernatant was discarded and washed five times with 500 μl IP-specific lysis buffer (cat. no. 26149; Thermo Fisher Scientific, Inc.). Finally, KLC3 and COL3A1 levels were analyzed by western blotting using anti-KLC3 (1:200; cat. no. ab180523; Abcam) and anti-COL3A1 (1:200; cat. no. 22734-1-AP; Proteintech Group, Inc.) antibodies.

Statistical analysis. Statistical analysis was conducted using SPSS 20.0 software (IBM Corp.) and GraphPad Prism version 8.0.2 (Dotmatics). Each experiment was performed in triplicate and continuous data are presented as the mean ± standard deviation. The differences between experimental groups were analyzed using one-way ANOVA followed by Bonferroni's post hoc test or unpaired two-tailed Student's t-test. Survival analysis was performed using the Kaplan-Meier method and log-rank test. $P<0.05$ was considered to indicate a statistically significant difference.

Results

KLC3 expression and survival analysis in OC. To assess the relationship between KLC3 and OC, the present study initially examined the expression of KLC3 in the GEPIA database, which revealed high mRNA levels of KLC3 in OC compared with normal tissue (Fig. 1A). Subsequently, the present study investigated the expression of KLC3 in the GSE12470 and GSE18520 datasets, and its expression was also significantly elevated in OC tissues compared with in tissues from healthy controls in these datasets (Fig. 1B and C). The Kaplan-Meier curve analysis demonstrated that patients with OC and low KLC3 expression had a better prognosis in different probesets: 1570402_at (HR=1.39, 95% CI 1.13-1.7) and 239853_at (HR=1.52, 95% CI 1.24-1.87) (Fig. 1D and E). Additionally, the results of IHC indicated that the expression of KLC3 was higher in OC tissues than that in normal tissues (Fig. 1F). Western blot analysis of five OC samples and five normal samples also revealed an elevated expression of KLC3 in OC (Fig. 1G). Finally, based on the expression levels of KLC3 in OC, 48 patients were categorized into high and low expression groups. The results revealed that patients with OC and high KLC3 expression had a poorer overall survival rate (Fig. 1H). Based on these findings, it could be hypothesized

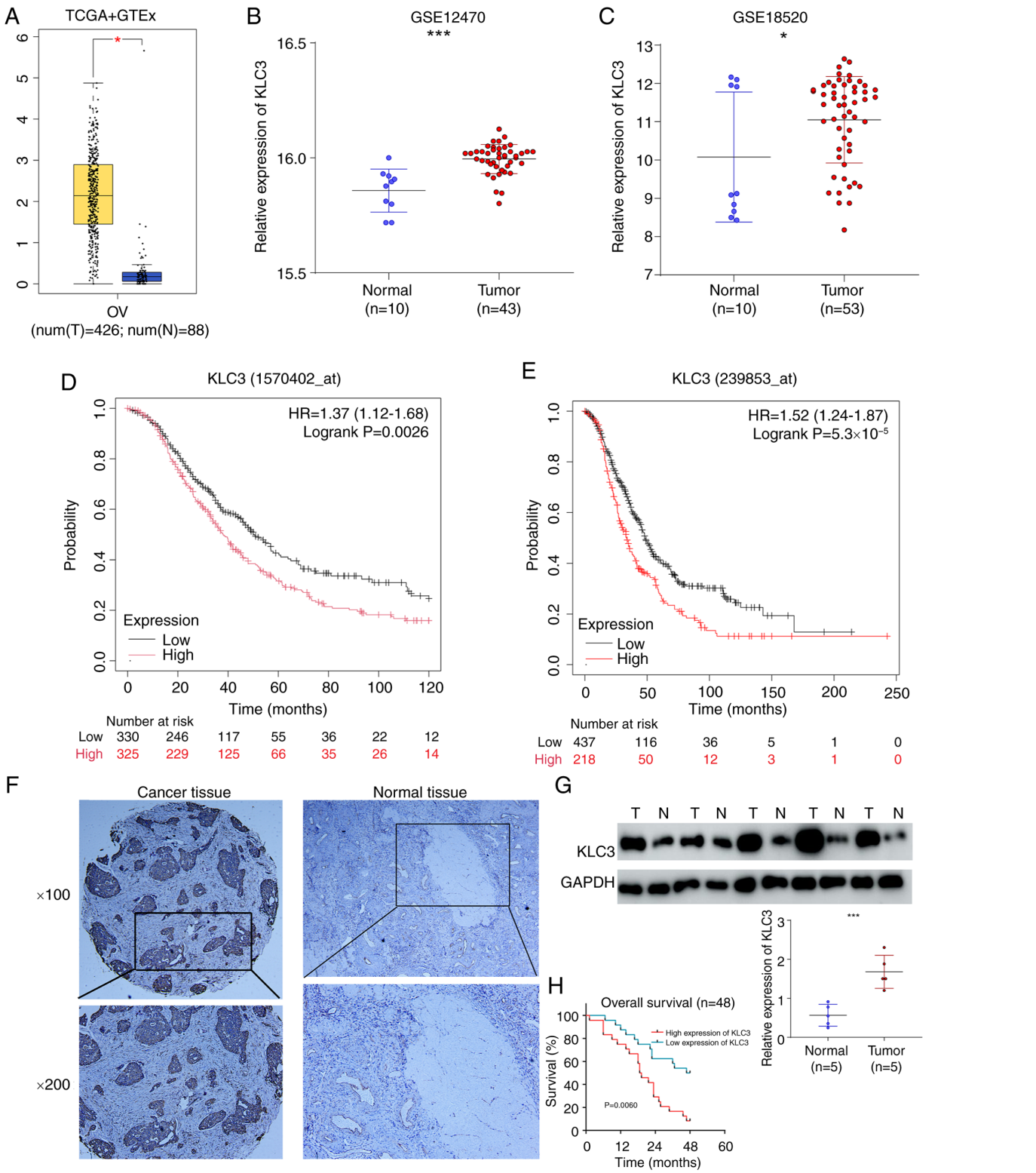

Figure 1. Bioinformatics analysis shows that KLC3 is highly expressed in OC tissues and is associated with poor prognosis. (A) KLC3 mRNA expression levels were determined by Gene Expression Profiling Interactive Analysis. Boxplot analysis shows the expression levels in log2 (TPM + 1). KLC3 mRNA levels in OC tissues and N ovarian tissues in the (B) GSE12470 and (C) GSE18520 datasets. Kaplan-Meier plotter database was used to assess the overall survival in different probes: (D) 1570402_at (HR=1.39, 95% CI 1.13-1.7, P=0.0017) and (E) 239853_at (HR=1.52, 95% CI 1.24-1.87, P=5.3x10^{-5}). (F) Representative immunohistochemical staining of KLC3 protein expression in OC and N ovarian tissues. (G) Western blot analysis of the protein levels of KLC3 in five OC tissues and five ovarian tissue. (H) Overall survival of all patients in relation to KLC3 expression. *P<0.05, ***P<0.001. GTEx, Genotype-Tissue Expression; KLC3, kinesin light chain 3; N, normal; OC, ovarian cancer; T, tumor; TCGA, The Cancer Genome Atlas.

that KLC3 serves a notable role in the development and progression of OC, warranting further investigation into its function.

Effect of KLC3 alterations on OC cell proliferation, migration, apoptosis and DNA damage repair capacity. The present study examined the mRNA and protein expression

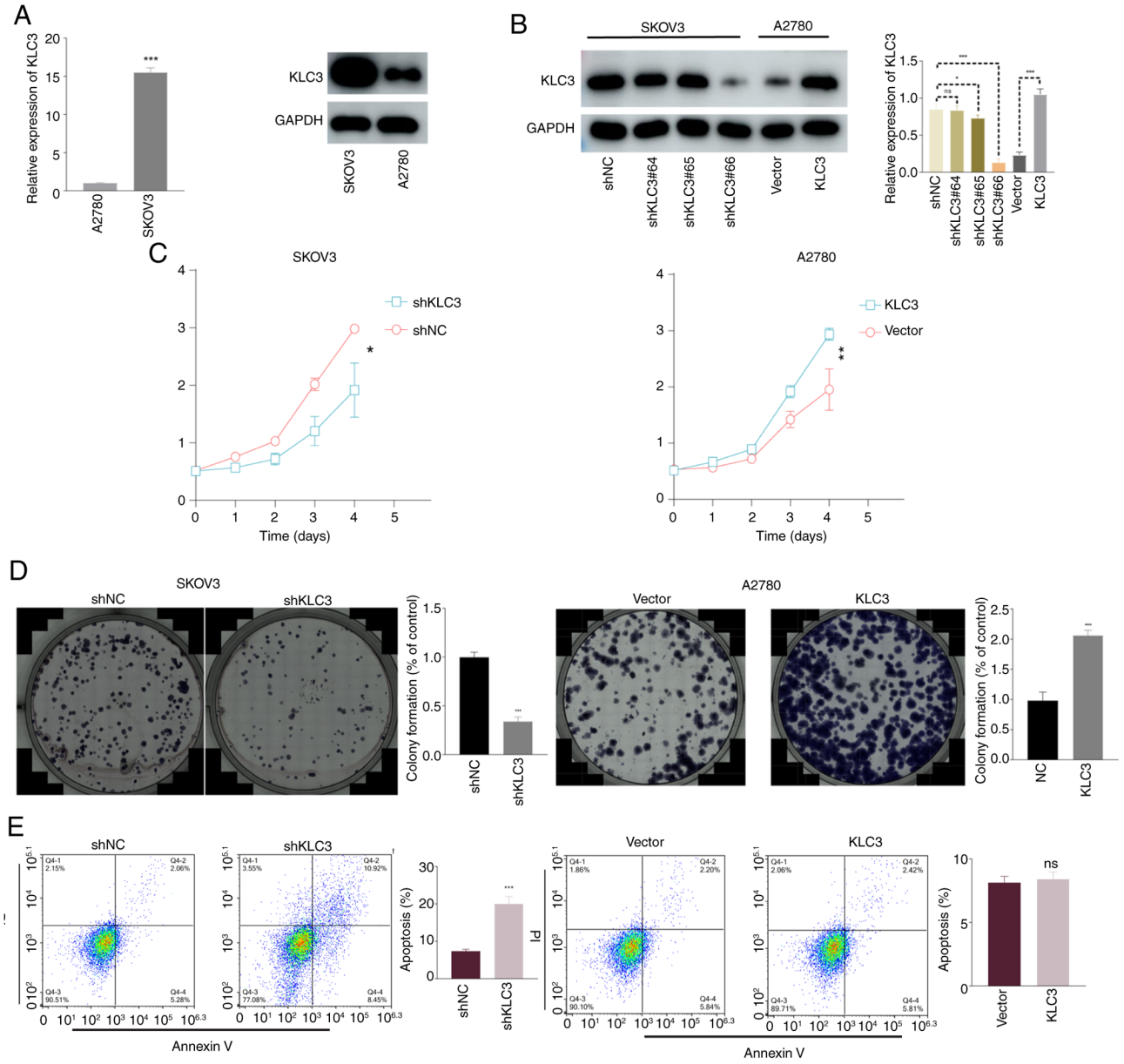

Figure 2. KLC3 promotes the proliferation of OC cells. (A) Reverse transcription-quantitative PCR and western blot analysis were performed to investigate the expression of KLC3 in different OC cell lines. (B) KLC3 was knocked down and overexpressed in SKOV3 and A2780 cells, and the knockdown and overexpression efficiency is verified by western blotting. (C) Cell Counting Kit-8 cell proliferation assay verified the proliferation of OC cells after KLC3 knockdown and overexpression. (D) Colony formation assay in OC cells with KLC3 knockdown and KLC3 overexpression (n=3). (E) Flow cytometric analysis of apoptosis after KLC3 knockdown or KLC3 overexpression. *P<0.05, **P<0.05, ***P<0.001. KLC3, kinesin light chain 3; NC, negative control; ns, not significant; OC, ovarian cancer; sh, short hairpin.

levels of KLC3 in two OC cell lines, SKOV3 and A2780. As shown in Fig. 2A, the expression of KLC3 was significantly higher in SKOV3 cells compared with that in A2780 cells. To investigate the functional role of KLC3 in OC, lentiviral knockdown of KLC3 was performed in the SKOV3 cell line and overexpression of KLC3 was induced in the A2780 cell line. Notably, shKLC3#66 exhibited optimal knockdown efficiency (subsequently denoted as shKLC3), achieving a knockdown rate of 80%, and the overexpression vector met the experimental standards for subsequent analyses (Fig. 2B).

To assess proliferation, the CCK-8 assay was performed over 5 consecutive days. The results revealed a significant reduction in proliferation following KLC3 knockdown, whereas proliferation was enhanced in response to KCL3 overexpression (Fig. 2C). The colony formation assay demonstrated diminished colony-forming ability following KCL3 knockdown relative to the control group, whereas this ability was enhanced post-KCL3 overexpression (Fig. 2D).

When investigating the relationship between KLC3 and apoptosis, it was revealed that knocking down KLC3 significantly increased the apoptosis of OC cells, whereas overexpression of KLC3 did not result in a noticeable change in apoptosis levels (Fig. 2E). Similarly, compared with in the control group, knockdown of KLC3 weakened the migratory ability of OC cells in the Transwell assay; however, overexpression of KLC3 did not lead to a significant change in the migratory ability of A2780 cells (Fig. 3A). In order to further investigate the underlying mechanisms, changes in

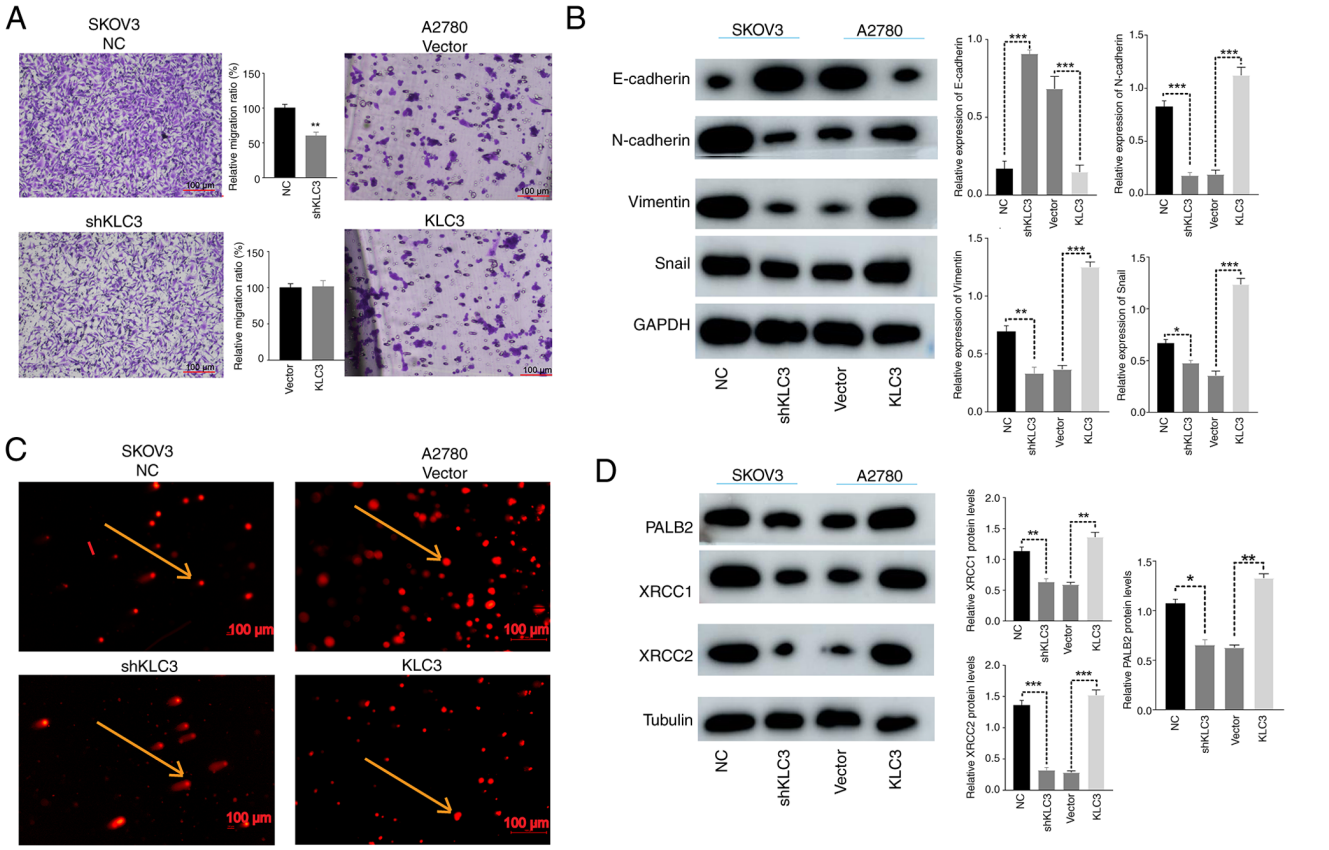

Figure 3. Effects of KLC3 on the migration and DNA damage of OC cells. (A) Migration of lung cancer cells was analyzed using a Transwell assay. Scale bar, 100 μm. (B) Expression levels of epithelial-mesenchymal transition-associated proteins in OC cells, detected by western blotting. (C) DNA double-strand breakage was observed using the comet assay. The cells indicated by arrows represent intact DNA strands (SKOV3 NC and A2780 Vector) and broken DNA strands (SKOV3 shKLC3 and A2780 KLC3). Scale bar, 100 μm. (D) Western blot analysis of XRCC1, XRCC2 and PALB2 expression. The mean grayscale of bands was semi-quantitatively analyzed. *P<0.05, **P<0.05, ***P<0.001. KLC3, kinesin light chain 3; NC, negative control; OC, ovarian cancer; sh, short hairpin.

EMT-related proteins, such as E-cadherin, N-cadherin, Snail and Vimentin, were examined through western blotting. It was observed that when the expression of KLC3 was knocked down, there was a corresponding decrease in the expression levels of N-cadherin, Snail and Vimentin, whereas an increase in E-cadherin expression was noted. Conversely, when KLC3 expression was increased, there was a concomitant increase in the expression levels of N-cadherin, Snail and Vimentin, with a decrease in E-cadherin expression (Fig. 3B).

DNA damage is a known instigator in the transformation of normal cells into tumor cells. In the context of cancer treatment, augmenting the efficacy of radiotherapy and chemotherapy involves impeding DNA damage repair in tumor cells through diverse modalities. The association between KLC3 expression and resistance to DNA damage in OC was substantiated through the comet assay. The reduced expression of KLC3 resulted in a marked increase in uncoiled and damaged DNA strands and fragments, whereas overexpression of KLC3 exhibited minimal impact on DNA damage (Fig. 3C). Examination of the DNA damage-associated proteins XRCC1, XRCC2 and PALB2 revealed that diminished expression of KLC3 corresponded to reduced expression levels of XRCC1, XRCC2 and PALB2; conversely, overexpression of KLC3 was associated with elevated levels of these proteins (Fig. 3D). These collective findings indicated that KLC3 may have a pivotal role in various malignant phenotypes, as well as anti-DNA damage repair mechanisms, within human OC cell lines.

KLC3 knockdown suppresses the in vivo growth of OC cells. The impact of KLC3 knockdown on tumor growth was assessed using a nude mouse xenograft model. Compared with in the control group, KLC3 knockdown impeded tumor growth (Fig. 4A), with a notably reduced growth rate compared with that in the control group (Fig. 4C). In addition, IHC analysis revealed decreased expression of KLC3 and its associated proliferation marker PCNA in the knockdown group (Fig. 4E). By contrast, overexpression of KLC3 stimulated *in vivo* tumor cell proliferation (Fig. 4B) and markedly increased tumor growth rate (Fig. 4D). The results of IHC indicated no significant difference in the expression levels of KLC3 and PCNA between the overexpression group and the control group (Fig. 4F). No difference in KLC3 expression was found after tumor formation; however, the overexpression efficiency of all cells was verified by western blotting before injection. These findings underscore the pivotal role of KLC3 in OC cell proliferation.

High-throughput sequencing analysis. According to the high-throughput sequencing analysis, a total of 13,516

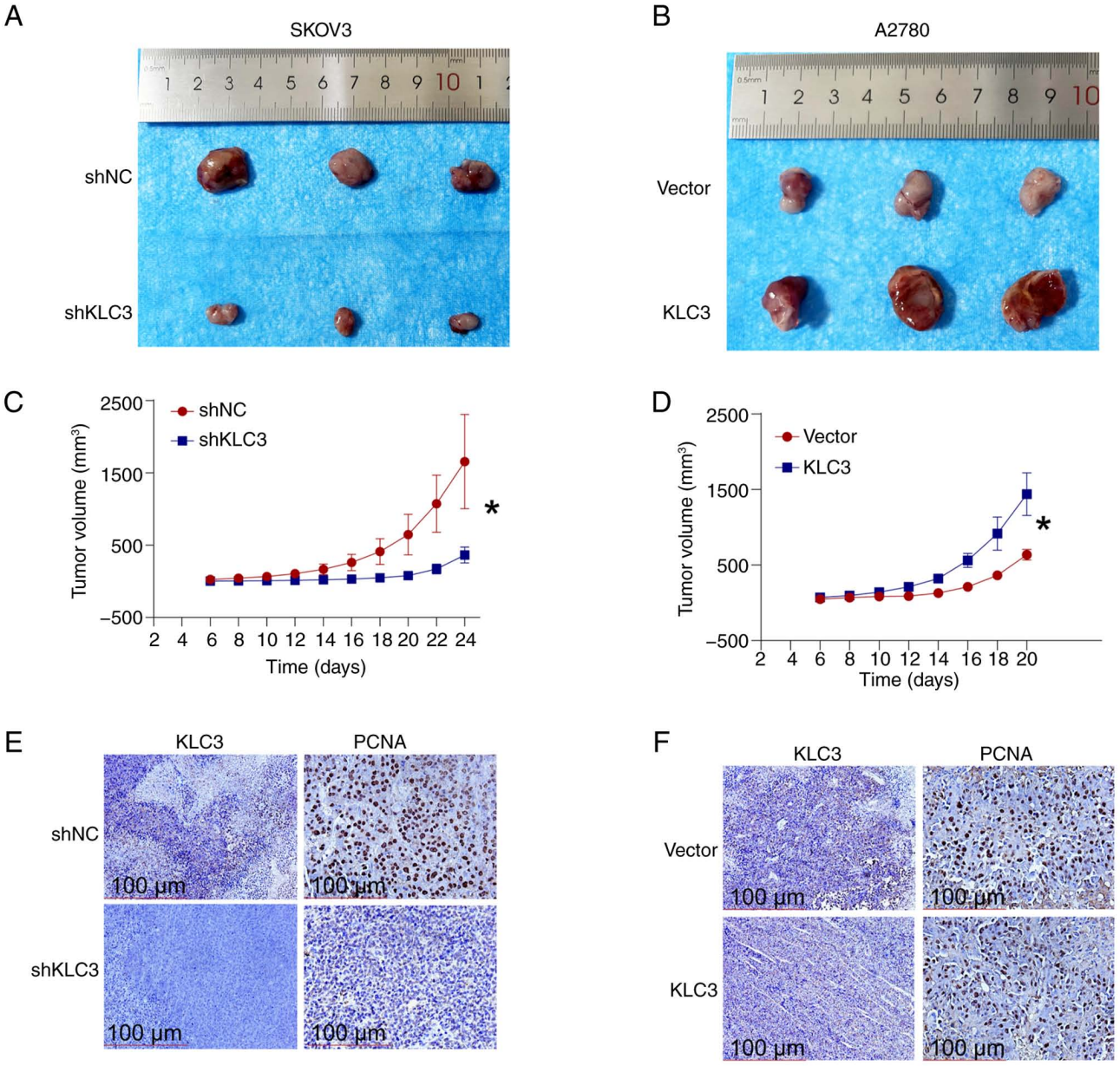

Figure 4. Knockdown of KLC3 effectively suppresses tumor growth in nude mice. Nude mice were subcutaneously injected with (A) shNC or shKLC3 SKOV3 cells. (B) Nude mice were subcutaneously injected with A2780 cells transfected with Vector or A2780 cells overexpressing KLC3. (C) Tumor sizes were measured after sizeable tumor formation (day 6) following shNC or shKLC3 SKOV3 cell injection. (D) Tumor sizes were measured after sizeable tumor formation (day 6) following injection with A2780 cells transfected with Vector or A2780 cells overexpressing KLC3. Inoculated mice were sacrificed on days 21(KLC3 and Vector groups) and 24(shNC and shKLC3 groups) and the tumors were excised for analysis (n=3). Representative immunohistochemical staining of KLC3 and PCNA in xenograft tumors from nude mice in the (E) shNC and shKLC3, and (F) Vector and KLC3 groups. Scale bar, 100 μm. KLC3, kinesin light chain 3; NC, negative control; sh, short hairpin. *P<0.05.

differentially expressed genes were identified between the SKOV3-NC and SKOV3-shKLC3 groups. The screening criteria were set at fold change ≥2 and P<0.05, resulting in 376 differentially expressed genes, with 261 upregulated and 115 downregulated (Fig. 5A and C). The top 10 downregulated genes were validated by PCR, and it was revealed that seven were significantly decreased and three showed no change between the shKLC3 and NC groups; COL3A1 exhibited the most significant difference (Fig. 5D). Western blotting results demonstrated that KLC3 knockdown led to decreased COL3A1 levels (Fig. 5E). Pathway enrichment analysis revealed that the 'PI3K-Akt signaling pathway' was the most enriched (8.57%), followed by the 'TNF signaling pathway' (7.43%) among others (Fig. 5B). The western blot analysis results for AKT, PI3K, p-AKT and p85α confirmed that decreased KLC3 expression did not affect the levels of AKT and PI3K, whereas it did lead to a decrease in p-AKT and p38a levels. Conversely, increased KLC3 expression did not impact the levels of AKT and PI3K, but resulted in an increase in p-AKT and p38a expression (Fig. 5F). Therefore, these findings suggested that overexpression of KLC3 may promote COL3A1 expression and activate the PI3K/AKT signaling pathway in OC cells.

KLC3 promotes activation of the PI3K/AKT pathway through COL3A1. The aforementioned findings demonstrated that alterations in KLC3 can lead to changes in COL3A1 and

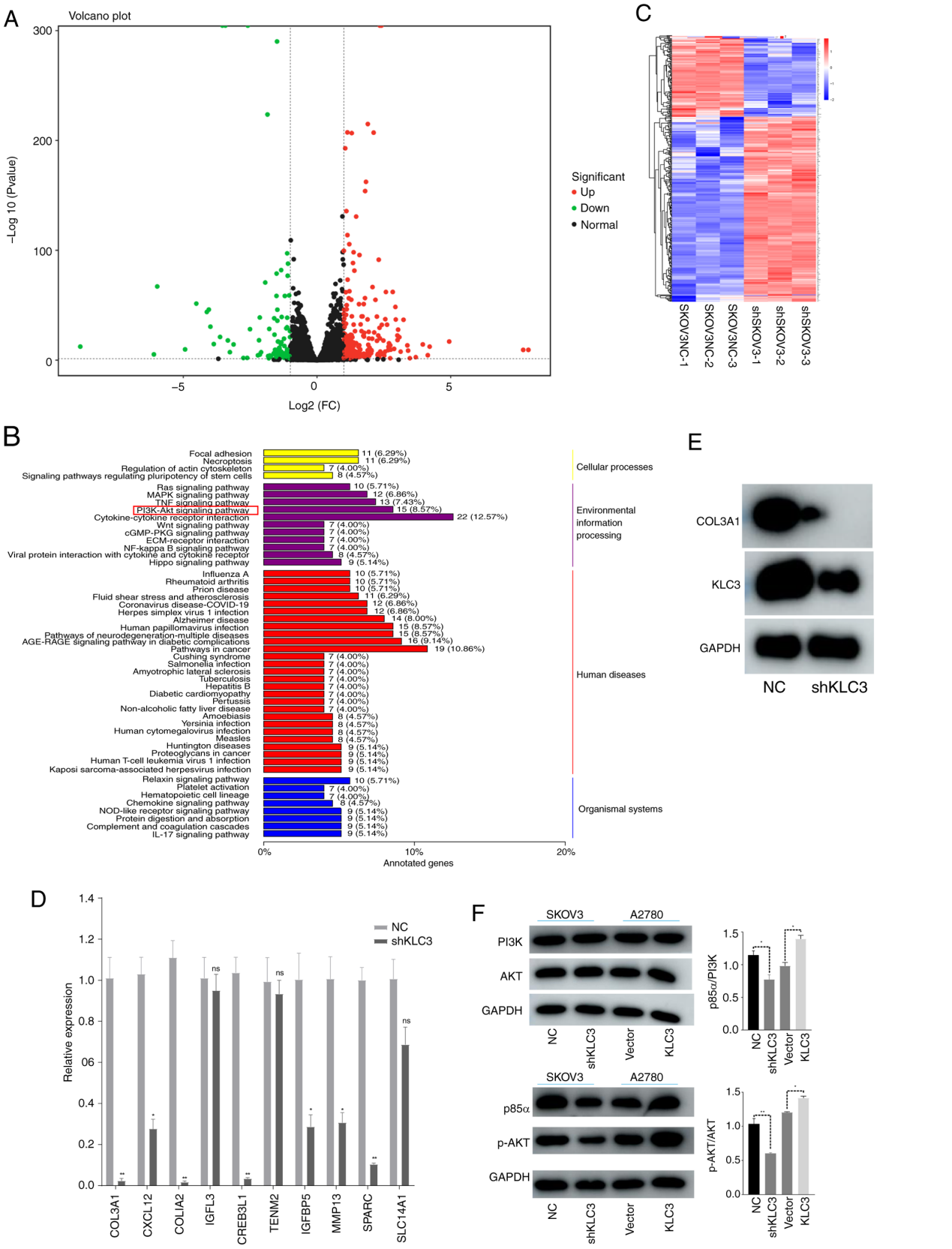

Figure 5. KLC3 activates the PI3K/AKT pathway in ovarian cancer. (A) Differential mRNA volcano plot. Green dots represent downregulated genes, while red dots represent upregulated genes. The abscissa is the FC. (B) KEGG classification diagram of differentially expressed genes. (C) Clustering diagram of differentially expressed genes. The horizontal axis represents sample names and clustering results, and the vertical axis represents differentially expressed genes and gene clustering results. Different columns represent different samples, and different rows represent different genes. The color represents the expression level of the gene in the sample. (D) Reverse transcription-quantitative PCR was used to verify the expression of the top 10 differentially expressed genes. (E) Western blotting was used to detect the changes in KLC3 and COL3A1 protein expression in SKOV3 cells. (F) Western blotting was used to investigate the changes in PI3K/AKT pathway proteins after KLC3 expression was altered. *P<0.05, **P<0.05 vs. NC or as indicated. COL3A1, collagen type III α1; FC, fold change; KEGG, Kyoto Encyclopedia of Genes and Genomes; KLC3, kinesin light chain 3; NC, negative control; ns, not significant; p-, phosphorylated; sh, short hairpin.

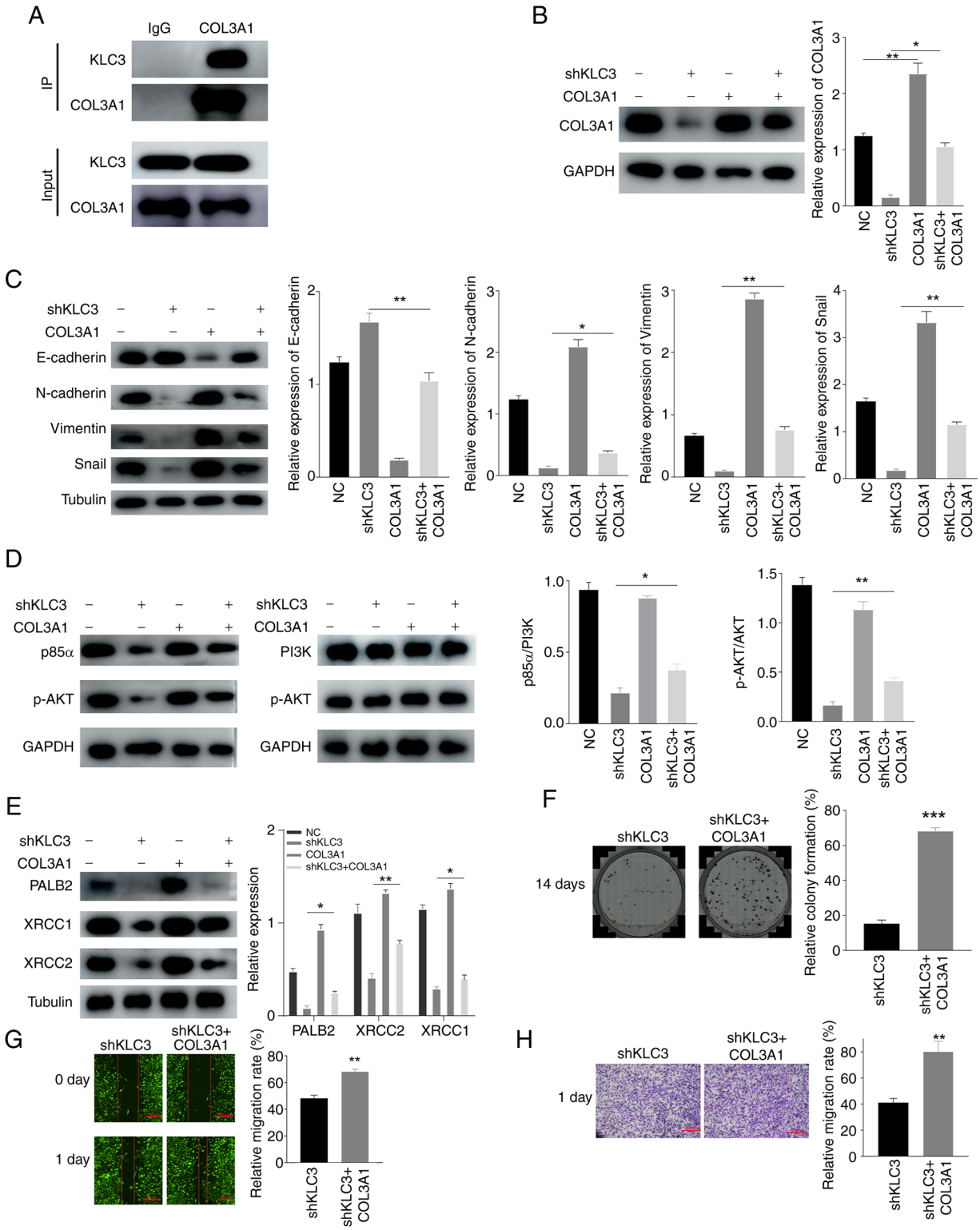

Figure 6. Effects of KLC3 knockdown on OC cells can be reversed by COL3A1 overexpression. (A) KLC3 and COL3A1 in SKOV3 cells can be co-immunoprecipitated. (B) Western blot analysis of COL3A1 expression. (C) Western blot analysis of epithelial-mesenchymal transition-related proteins. (D) Western blot analysis of PI3K/AKT signaling pathway proteins. (E) Western blot analysis of PALB2, XRCC1 and XRCC2 expression. (F) Recovery experiment of the changes in proliferation of OC cells after knocking down KLC3 and overexpressing COL3A1. (G) Recovery of OC cell migration after knockdown of KLC3 and overexpression of COL3A1. (H) Migratory ability of OC cells was observed by Transwell assay. *P<0.05, **P<0.01, ***P<0.001 vs. shKLC3 or as indicated. COL3A1, collagen type III α1; IP, immunoprecipitation; OC, ovarian cancer; KLC3, kinesin light chain 3; NC, negative control; ns, not significant; p-, phosphorylated; sh, short hairpin.

activation of the PI3K/AKT pathway. To further investigate the mechanism by which KLC3 promotes the malignant progression of OC cells, the interaction between KLC3 and COL3A1 was examined using co-IP. The results revealed that there was an interaction between KLC3 and COL3A1 in SKOV3 cells (Fig. 6A). Furthermore, overexpression of COL3A1 in SKOV3

cells and in shKLC3-infected cells resulted in alterations in the expression of DNA damage-related genes and EMT-related genes; the expression levels of XRCC1, XRCC2, PALB2, N-cadherin, Snail and Vimentin were increased, whereas E-cadherin expression was decreased compared with in the shKLC3 group (Fig. 6B, C and E). Following overexpression of COL3A1, similar effects were observed when comparing it to knocking down KLC3 alone. Similarly, the overexpression of COL3A1 stimulated activation of the PI3K/AKT pathway, and overexpression of COL3A1 reversed the inhibitory effects of shKLC3 (Fig. 6D). The results of clonogenic (Fig. 6F), wound healing (Fig. 6G) and Transwell (Fig. 6H) assays revealed that the migratory and proliferative capabilities were increased in the shKLC3 + COL3A1 group compared with those in the shKLC3 group. These findings suggested that KLC3 may activate the PI3K/AKT pathway by interacting with COL3A1 and could contribute to the malignant functions of OC cells.

Discussion

In eukaryotic cells, the transportation of all structures to specific locations at precise times relies on microtubules, with kinesin proteins providing essential energy for this process (23). Aberrant expression of kinesin proteins has been reported to be linked to various types of cancer, including OC, and is associated with prognosis, proliferation, metastasis and drug resistance (24-27). Additionally, kinesin proteins serve a pivotal role in diverse biological processes within tumors by participating in the gene transcription and translation, and division of tumor cells (25). In recent years, kinesin proteins have garnered notable attention as a novel target for tumor therapy (5-12). However, the association between KLC3 and tumors has been relatively understudied, particularly in relation to OC. In the present study, data from the GEPIA and GEO databases revealed high expression levels of KLC3 in OC. Furthermore, Kaplan-Meier plotter analysis demonstrated that higher KLC3 expression levels were associated with a poorer prognosis in patients with OC.

In the present study, western blot analysis was employed to validate the expression of KLC3 in five normal ovarian tissue samples and five OC samples. The overall expression of KLC3 was revealed to be significantly higher in OC tissues compared with that in normal tissues. Subsequently, IHC was utilized to evaluate the protein expression of KLC3 in OC specimens. The experimental findings demonstrated an upregulation of KLC3 in OC tissues. Based on the differential expression levels of KLC3 in OC tissues, patients were stratified into high and low expression groups. Patients with lower KLC3 expression exhibited a more favorable prognosis, which was consistent with the results of bioinformatics analysis. Unfortunately, owing to the limited availability of OC samples, the present study was unable to amass a sufficient number of samples to validate the association between KLC3 expression and clinical characteristics. Future studies should aim to increase the sample size to address this limitation. These collective findings suggested that KLC3 may represent a novel oncogene in OC.

EMT has a crucial role in embryonic morphogenesis, and confers tumor cells with motility, stemness, drug resistance and microenvironmental adaptability during cancer progression (28). Early dissemination is a hallmark of OC, where metastasizing cancer cells undergo diverse transformation patterns, such as acquiring mesenchymal characteristics closely associated with EMT. Furthermore, the hematogenous and lymphatic spread of advanced-stage OC cells is intricately linked to EMT (29,30). Previous research has indicated the involvement of certain members of the motor protein family in EMT (9). Building on this knowledge, the current study investigated the association between KLC3 and EMT in OC. The findings revealed that alterations in KLC3 led to changes in the expression levels of proteins related to EMT progression, including N-cadherin, Snail, Vimentin and E-cadherin; thus confirming that overexpression of KLC3 may enhance the process of EMT in OC cells.

Enhanced radioresistance of lung cancer cells has been demonstrated to be associated with the overexpression of KLC2 and KLC4, which is considered to be linked to anti-DNA damage mechanisms. Additionally, KLC4 deficiency has been shown to trigger the DNA damage response (6,7). Building on these findings, the present study investigated the association between KLC3 and DNA damage. The comet assay results revealed that downregulation of KLC3 led to an increase in DNA damage in OC cells, thus indicating a notable association between KLC3 and OC cell resistance to DNA damage.

The COL3A1 protein is predominantly present in stromal cells and is primarily synthesized by fibroblasts, contributing to the development of extracellular matrix, cellular adhesion and tissue remodeling processes (31). Previous research has indicated an upregulation of COL3A1 mRNA expression in various tumors, such as breast cancer, lung cancer, gastric cancer, OC and esophageal cancer (32). Elevated levels of COL3A1 have been linked to increased proliferation, invasion, migration and drug resistance in multiple tumor types, including OC (33-36). RNA-seq technology has been extensively utilized for fundamental research purposes, as well as clinical diagnostics and pharmaceutical advancements (37). In the present study, RNA-seq analysis was employed to identify alterations in gene expression within the SKOV3 OC cell line following KLC3 downregulation. The findings were subsequently validated through RT-qPCR analysis and western blotting, alongside a literature review. Additionally, co-IP experiments confirmed the interaction between KLC3 and COL3A1, ultimately establishing COL3A1 as a downstream target of KLC3. Furthermore, sequencing results highlighted significant enrichment of the PI3K/AKT pathway. It is well-established that activation of PI3K/AKT promotes metastasis in OC (38,39), while also inhibiting apoptosis through DNA repair mechanisms and promoting drug resistance (40,41). Building upon this foundation, the present study explored the relationship between KLC3 and the PI3K/AKT signaling pathway in OC, and revealed that reduced KLC3 expression did not impact PI3K or AKT levels but led to decreased p85α and p-AKT expression; conversely overexpression of KLC4 activated this pathway. Collectively these findings indicated the involvement of KLC4 in OC progression with implications for EMT processes and DNA damage.

After knocking down KLC3 and overexpressing COL3A1 in SKOV3 OC cells, an increase in the expression levels of

N-cadherin, Snail and Vimentin was detected compared with in the knockdown group, whereas E-cadherin expression was decreased. Additionally, XRCC1, XRCC2 and PALB2 exhibited increased expression compared with in the knockdown group. These results suggested that the overexpression of COL3A1 could partially mitigate the weakened malignant function of OC cells caused by reduced KLC3 expression.

In conclusion, the findings of the present study indicated that KLC3 may facilitate the PI3K/AKT signaling pathway, and promote the proliferation and migration of OC cells via COL3A1. These findings suggested a novel mechanism of action for KLC3 in the pathogenesis of OC, thus highlighting its potential as a promising target for OC therapy.

Acknowledgements

Not applicable.

Funding

The present study was supported by The Gansu Province Health Industry Scientific Research Plan Project (grant no. GSWSHL2022_34).

Availability of data and materials

The RNA-seq data generated in the present study may be found in the Sequence Read Archive under accession number PRJNA1137301 or at the following URL: https://www.ncbi.nlm.nih.gov/sra/?term=PRJNA1137301. The other data generated in the present study may be requested from the corresponding author.

Authors' contributions

JY and YL designed the present study. XZ analyzed the data and wrote the manuscript. ML, XW and XL collected the data. RH, XL and ML analyzed the data. YL revised the manuscript. JY and YL confirm the authenticity of all the raw data. All authors read and approved the final version of the manuscript.

Ethics approval and consent to participate

The use of patient tissues was approved by the Institutional Ethics Committee of The First Hospital of Lanzhou University (approval no. LDYYLL-2019-279). Written informed consent was obtained from the patients prior to sample collection. *In vivo* experiments were conducted with the approval of the Animal Experimental Ethics Committee of The First Hospital of Lanzhou University of (approval no. LDYYLL-2023-495).

Patient consent for publication

Not applicable.

Competing interests

The authors declare that they have no competing interests.

References

1. Cui W, Rocconi RP, Thota R, Anderson RA, Bruinooge SS, Comstock IA, Denduluri N, Gassman A, Gralow J, Hutt KJ, *et al*: Measuring ovarian toxicity in clinical trials: An American society of clinical oncology research statement. Lancet Oncol 24: e415-e423, 2023.
2. Godbole N, Quinn A, Carrion F, Pelosi E and Salomon C: Extracellular vesicles as a potential delivery platform for CRISPR-Cas based therapy in epithelial ovarian cancer. Semin Cancer Biol 96: 64-81, 2023.
3. Rayment I: Kinesin and myosin: Molecular motors with similar engines. Structure 4: 501-504, 1996.
4. Zhong M, Gong L, Li N, Guan H, Gong K, Zhong Y, Zhu E, Wang X, Jiang S, Li J, *et al*: Pan-cancer analysis of kinesin family members with potential implications in prognosis and immunological role in human cancer. Front Oncol 13, 1179897, 2023.
5. Qiao S, Jiang Y, Li N and Zhu X: The kinesin light chain-2, a target of mRNA stabilizing protein HuR, inhibits p53 protein phosphorylation to promote radioresistance in NSCLC. Thorac Cancer 14: 1440-1450, 2023.
6. Baek JH, Yun HS, Kim JY, Lee J, Lee YJ, Lee CW, Song JY, Ahn J, Park JK, Kim JS, *et al*: Kinesin light chain 4 as a new target for lung cancer chemoresistance via targeted inhibition of checkpoint kinases in the DNA repair network. Cell Death Dis 11: 398, 2020.
7. Baek JH, Lee J, Yun HS, Lee CW, Song JY, Um HD, Park JK, Park IC, Kim JS, Kim EH and Hwang SG: Kinesin light chain-4 depletion induces apoptosis of radioresistant cancer cells by mitochondrial dysfunction via calcium ion influx. Cell Death Dis 9: 496, 2018.
8. Feng S, Luo S, Ji C and Shi J: miR-29c-3p regulates proliferation and migration in ovarian cancer by targeting KIF4A. World J Surg Oncol 18: 315, 2020.
9. Sheng N, Xu YZ, Xi QH, Jiang HY, Wang CY, Zhang Y and Ye Q: Overexpression of KIF2A is suppressed by miR-206 and associated with poor prognosis in ovarian cancer. Cell Physiol Biochem 50: 810-822, 2018.
10. Li H, Zhang W, Sun X, Chen J, Li Y, Niu C, Xu B and Zhang Y: Overexpression of kinesin family member 20A is associated with unfavorable clinical outcome and tumor progression in epithelial ovarian cancer. Cancer Manag Res 10: 3433-3450, 2018.
11. Kawai Y, Shibata K, Sakata J, Suzuki S, Utsumi F, Niimi K, Sekiya R, Senga T, Kikkawa F and Kajiyama H: KIF20A expression as a prognostic indicator and its possible involvement in the proliferation of ovarian clear-cell carcinoma cells. Oncol Rep 40: 195-205, 2018.
12. Han X, Yang L, Tian H and Ji Y: Machine learning developed a PI3K/Akt pathway-related signature for predicting prognosis and drug sensitivity in ovarian cancer. Aging (Albany NY) 15: 11162-11183, 2023.
13. Konjikusic MJ, Gray RS and Wallingford JB: The developmental biology of kinesins. Dev Biol 469: 26-36, 2021.
14. Yu L, Wei J and Liu P: Attacking the PI3K/Akt/mTOR signaling pathway for targeted therapeutic treatment in human cancer. Semin Cancer Biol 85: 69-94, 2022.
15. Li H, Zeng J and Shen K: PI3K/AKT/mTOR signaling pathway as a therapeutic target for ovarian cancer. Arch Gynecol Obstet 290: 1067-1078, 2014.
16. Ediriweera MK, Tennekoon KH and Samarakoon SR: Role of the PI3K/AKT/mTOR signaling pathway in ovarian cancer: Biological and therapeutic significance. Semin Cancer Biol 59: 147-160, 2019.
17. Yoshihara K, Tajima A, Komata D, Yamamoto T, Kodama S, Fujiwara H, Suzuki M, Onishi Y, Hatae M, Sueyoshi K, *et al*: Gene expression profiling of advanced-stage serous ovarian cancers distinguishes novel subclasses and implicates ZEB2 in tumor progression and prognosis. Cancer Sci 100: 1421-1428, 2009.
18. Mok SC, Bonome T, Vathipadiekal V, Bell A, Johnson ME, Wong KK, Park DC, Hao K, Yip DK, Donninger H, *et al*: A gene signature predictive for outcome in advanced ovarian cancer identifies a survival factor: Microfibril-associated glycoprotein 2. Cancer Cell 16: 521-532, 2009.
19. O'Shea AS: Clinical staging of ovarian cancer. Methods Mol Biol 2424: 3-10, 2022.
20. Dixon JR Jr: The International conference on harmonization good clinical practice guideline. Qual Assur 6: 65-74, 1998.

21. Livak KJ and Schmittgen TD: Analysis of relative gene expression data using real-time quantitative PCR and the 2(-Delta Delta C(T)) Method. Methods 25: 402-408, 2001.
22. Zhou Y, Zhou B, Pache L, Chang M, Khodabakhshi AH, Tanaseichuk O, Benner C and Chanda SK: Metascape provides a biologist-oriented resource for the analysis of systems-level datasets. Nat Commun 10: 1523, 2019.
23. Tjioe M, Shukla S, Vaidya R, Troitskaia A, Bookwalter CS, Trybus KM, Chemla YR and Selvin PR: Multiple kinesins induce tension for smooth cargo transport. Elife 8: e50974, 2019.
24. Cong S, Fu Y, Zhao X, Guo Q, Liang T, Wu D, Wang J and Zhang G: KIF26B and CREB3L1 derived from immunoscore could inhibit the progression of ovarian cancer. J Immunol Res 2024: 4817924, 2024.
25. Liu X, Gong H and Huang K: Oncogenic role of kinesin proteins and targeting kinesin therapy. Cancer Sci 104: 651-656, 2013.
26. Li X, Huang W, Huang W, Wei T, Zhu W, Chen G and Zhang J: Kinesin family members KIF2C/4A/10/11/14/18B/20A/23 predict poor prognosis and promote cell proliferation in hepatocellular carcinoma. Am J Transl Res 12: 1614-1639, 2020.
27. Liang LY and Li GS: The Roles of KIFC1 in the development of osteosarcoma: Characterization of potential therapeutic targets. Comput Math Methods Med 2022: 5039134, 2022.
28. Zhang G, Hou S, Li S, Wang Y and Cui W: Role of STAT3 in cancer cell epithelial-mesenchymal transition (Review). Int J Oncol 64: 48, 2024.
29. Śliwa A, Szczerba A, Pięta PP, Białas P, Lorek J, Nowak-Markwitz E and Jankowska A: A recipe for successful metastasis: Transition and migratory modes of ovarian cancer cells. Cancers (Basel) 16: 783, 2024.
30. Szczerba A, Śliwa A, Pieta PP and Jankowska A: The role of circulating tumor cells in ovarian cancer dissemination. Cancers(Basel) 14: 6030, 2022.
31. Kuivaniemi H and Tromp G: Type III collagen (COL3A1): Gene and protein structure, tissue distribution, and associated diseases. Gene 707: 151-171, 2019.
32. Zhang H, Ding C, Li Y, Xing C, Wang S, Yu Z, Chen L, Li P and Dai M: Data mining-based study of collagen type III alpha 1 (COL3A1) prognostic value and immune exploration in pan-cancer. Bioengineered 12: 3634-3646, 2021.
33. Januchowski R, Świerczewska M, Sterzyńska K, Wojtowicz K, Nowicki M and Zabel M: Increased expression of several collagen genes is associated with drug resistance in ovarian cancer cell lines. J Cancer 7: 1295-1310, 2016.
34. Xu W, Li Z, Zhu X, Xu R and Xu Y: miR-29 family inhibits resistance to methotrexate and promotes cell apoptosis by targeting COL3A1 and MCL1 in osteosarcoma. Med Sci Monit 24: 8812-8821, 2018.
35. Wang L, Sun Y, Guo Z and Liu H: COL3A1 overexpression associates with poor prognosis and cisplatin resistance in lung cancer. Balkan Med J 39: 393-400, 2022.
36. Gao YF, Zhu T, Chen J, Liu L and Ouyang R: Knockdown of collagen α-1(III) inhibits glioma cell proliferation and migration and is regulated by miR128-3p. Oncol Lett 16: 1917-1923, 2018.
37. Ozsolak F and Milos PM: RNA sequencing: Advances, challenges and opportunities. Nat Rev Genet 12: 87-98, 2011.
38. Wang H, Xu YH and Guo Y: Novel prognostic marker TGFBI affects the migration and invasion function of ovarian cancer cells and activates the integrin αvβ3-PI3K-Akt signaling pathway. J Ovarian Res 17: 50, 2024.
39. Li GW, Jin YP, Qiu JP and Lu XF: ITGB2 fosters the cancerous characteristics of ovarian cancer cells through its role in mitochondrial glycolysis transformation. Aging (Albany NY) 16: 3007-3020, 2024.
40. Ma S, Wang J, Cui Z, Yang X, Cui X, Li X and Zhao L: HIF-2α-dependent TGFBI promotes ovarian cancer chemoresistance by activating PI3K/Akt pathway to inhibit apoptosis and facilitate DNA repair process. Sci Rep 14: 3870, 2024.
41. Li W, Zhang K, Wang W, Liu Y, Huang J, Zheng M, Li L, Zhang X, Xu M, Chen G, *et al*: Combined inhibition of HER2 and VEGFR synergistically improves therapeutic efficacy via PI3K-AKT pathway in advanced ovarian cancer. J Exp Clin Cancer Res 43: 56, 2024.